Effect of final state interactions on particle production in d + Au collisions at energies available at the BNL Relativistic Heavy Ion Collider

Xiaoping Zhang,[1,2,3,*] Jinhui Chen,[4] Zhongzhou Ren,[1] N. Xu,[2] Zhangbu Xu,[5] Qiang Zheng,[6] and Xianglei Zhu[3]

[1]*Department of Physics, Nanjing University, Nanjing 210008, China*
[2]*Nuclear Science Division, Lawrence Berkeley National Laboratory, Berkeley, California 94720, USA*
[3]*Department of Engineering Physics, Tsinghua University, Beijing 100084, China*
[4]*Shanghai Institute of Applied Physics, CAS, Shanghai, 201800, China*
[5]*Brookhaven National Laboratory, Upton, New York 11973, USA*
[6]*School of Mathematics and Computer Science, Guizhou Normal University, Guiyang, 550001, China*

We show that particle species dependence of enhanced hadron production at intermediate transverse momentum (p_T) for d + Au collisions at RHIC can be understood in terms of the hadronization from string fragmentation and the subsequent hadronic rescatterings in the final state. A multiphase transport model (AMPT) with two different hadronization mechanisms, string fragmentation or parton coalescence, is used in our study. When the hadrons are formed from string fragmentation, the subsequent hadronic rescatterings will result in particle mass dependence of the nuclear modification factor R_{CP}, which is consistent with the present experimental data. On the other hand, in the framework of parton coalescence, the mass dependence disappears and the strangeness plays an important role in hadron production.

PACS number(s): 25.75.Dw, 24.10.Jv

The Cronin effect, which refers to the enhanced hadron production at intermediate transverse momentum (p_T) with increasing target nucleus size in proton-nucleus (pA) collisions, was first observed by Cronin *et al.* [1,2] in 1975 at center-of-mass energy $\sqrt{s_{NN}} = 27.4$ GeV. Recent experimental data in d + Au collisions from the Relativistic Heavy Ion Collider (RHIC) at Brookhaven National Laboratory have shown that a similar effect exists at a higher collision energy ($\sqrt{s} = 200$ GeV) [3,4]. An adequate understanding of the Cronin effect becomes especially important for making reliable theoretical interpretations of the observations in heavy ion collisions at RHIC, in which the quark-gluon plasma (QGP) is thought to be created [5]. Traditional explanations of the Cronin effect all involve multiple scattering of incoming partons before the hard scattering that leads to an enhancement at intermediate p_T [6–11]. The models can reproduce the observed centrality dependence for pions very well. However, none of these initial state models would predict a species-dependent Cronin effect, as the initial state parton scattering precedes fragmentation into the different hadronic species [4]. This may suggest that final state interactions (FSIs) would possibly contribute to the Cronin effect.

The final state effects depend on different hadronization mechanisms. In the parton recombination model, one mainly considers the final state parton scattering as a final state effect [12]. However, if one utilizes a string fragmentation hadronization model such as in the Lund string model [13,14], HIJING [15], and AMPT [16,17], since the minijet parton density after hard scattering is very small in d + Au collisions [17], the subsequent hadronic rescatterings after hadron formation would be the dominate part of final state effects in the d + Au system. Recently, Hwa and Yang [12] demonstrated that the recombi-

nation of soft and shower partons in the final state could explain the mass-dependent Cronin effect. This model predicts a larger enhancement for protons than for pions at $1 < p_T < 4$ GeV/c. However, the inclusion of quark recombination requires a high enough phase space density of partons [18], which may not be justified in d + Au collisions. Depending on the slope and the absolute value of the phase space distribution of partons, an alternate way for hadronization, i.e., string fragmentation, may take over [13–18]. In this scenario, hadrons are formed from the decay of excited strings, which results from the recombination of energetic minijet partons and soft strings that are produced from initial soft nucleon-nucleon interactions. After the hadronization, the subsequent hadronic rescatterings between formed hadrons or between formed hadrons and nucleon spectators should also be taken into account.

In this Rapid Communication we study quantitatively how the two different hadronization mechanisms (string fragmentation and parton coalescence) and the subsequent hadronic rescatterings would contribute to the nuclear modification factors in d + Au collisions at $\sqrt{s} = 200$ GeV. A multiphase transport model (AMPT) [16,17] with two versions, default (hadronization from Lund string fragmentation, mainly hadronic rescatterings in the final state, version 1.11) and string melting (hadronization from quark coalescence, version 2.11), are used to study the later-stage effect. The final state hadronic and/or partonic interactions are included in the calculations. Quark transverse momentum kicks due to multiple scatterings are treated in the same way as in Ref. [15]. Here, we assume no extra quark intrinsic p_T broadening [8] and see how the final state interactions would contribute to the observed Cronin effect. We show that recent data on particle species dependence of the central-to-peripheral nuclear modification factor R_{CP} at midrapidity for d + Au collisions at RHIC can be understood in terms of the hadronization from string fragmentation and the subsequent hadronic rescatterings in the final state.

---
[*]xpzhangnju@gmail.com

The AMPT model [16,17] is a hybrid model that consists of four main components: the initial conditions, the partonic interactions, conversion from the partonic to the hadronic matter, and the hadronic interactions. The initial conditions, which include the spatial and momentum distributions of hard minijet partons and soft string excitations, are obtained from the HIJING model (version 1.383 for this study). One uses a Woods-Saxon radial shape for the colliding gold nuclei and introduces a parametrized nuclear shadowing function that depends on the impact parameter of the collision. The ratio of quark structure function is parametrized as the following impact-parameter-dependent but Q^2 (and flavor)-independent form [16]

$$
\begin{aligned}
R_A(x, r) &\equiv \frac{f_a^A(x, Q^2, r)}{A f_a^N(x, Q^2)} \\
&= 1 + 1.19 \ln^{1/6} A (x^3 - 1.2x^2 + 0.21x) \\
&\quad - \left[\alpha_A(r) - \frac{1.08(A^{1/3} - 1)\sqrt{x}}{\ln(A + 1)}\right] e^{-x^2/0.01},
\end{aligned} \tag{1}
$$

where x is the light-cone momentum fraction of parton a, and f_a is the parton distribution function. The impact-parameter dependence of the nuclear shadowing effect is controlled by

$$
\alpha_A(r) = 0.133(A^{1/3} - 1)\sqrt{1 - r^2/R_0^2}, \tag{2}
$$

with r denoting the transverse distance of an interacting nucleon from the center of the nucleus with radius $R_0 = 1.2A^{1/3}$. The structure of the deuteron is described by the Hulthen wave function. Scatterings among partons are modeled by Zhang's parton cascade (ZPC) [19], which at present includes only two-body elastic scatterings with cross sections obtained from the perturbative quantum chromodynamics (pQCD) with screening masses. In the default AMPT model, after partons stop interacting, they recombine with their parent strings, which are produced from initial soft nucleon-nucleon interactions. The resulting strings are converted to hadrons using the Lund string fragmentation model. In case of string melting, the hadrons produced from string fragmentation are converted instead to their valence quarks and antiquarks. The subsequent partonic interactions are modeled by ZPC. After the partons freeze-out, they are recombined into hadrons through a quark coalescence process. The dynamics of the subsequent hadronic matter is described by a hadronic cascade, which is based on a relativistic transport model (ART) [20]. Final hadronic observables including contributions from the strong decays of resonances are determined when the hadronic matter freezes out.

We learn that Lin and Ko have done a study [17] on the global properties of deuteron-gold collisions with the default AMPT model, which shows good agreement with later experimental data [21,22]. Their study on nuclear effects is up to $p_T = 2$ GeV/c. Here we focus on the intermediate to higher p_T range where the Cronin effect exists. We study the deuteron-gold collisions at $\sqrt{s_{NN}} = 200$ GeV. The string fragmentation parameters are chosen to be the same as in Ref. [17]. The partonic scattering cross section is chosen to be 3 mb. The events are separated into different centrality
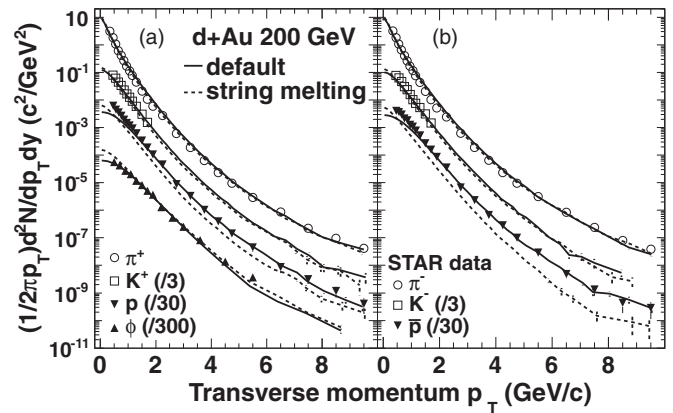

FIG. 1. Transverse momentum spectra of midrapidity ($|y| < 0.5$) pions, kaons, protons, and ϕ mesons in "minimum bias" $d + $Au collisions from default AMPT (solid lines) and string melting AMPT (dashed lines) vs data from the STAR Collaboration (statistical error only) [3,23].

bins using the number of participant nucleons suffering inelastic collisions. Figure 1 shows the midrapidity ($|y| < 0.5$) transverse momentum spectra of pions, kaons, protons, and ϕ mesons for "minimum bias" $d + $Au collisions from default AMPT (solid line) and string melting (dashed line). It is seen that both default and string melting AMPT can reproduce the $\pi^\pm$ and $K^\pm$ spectra well. For proton and antiproton production, the default version works well for $p_T > 1$ GeV/c, but underestimates the low p_T proton and antiproton yields. The string melting version underestimates the proton and antiproton production in the whole p_T range. For the ϕ meson spectrum, the default version works well in the whole p_T range, while the string melting one overestimates the low p_T ϕ meson yields in the "minimum bias" $d + $Au collisions.

To study the final state effect on the nuclear modification factor $R_{\rm CP}$, we first calculate the $R_{\rm CP}$ (0%–20%/40%–100% centrality) of different hadrons without including the final state hadronic interactions and resonance decays in the default AMPT. The $R_{\rm CP}$, which compares particle yield from central collisions to that of peripheral collisions, is defined as the ratio of particle yields in central collisions over those in peripheral ones scaled by the number of inelastic binary collisions $N_{\rm bin}$, that is,

$$
R_{\rm CP} = \frac{[dN/(N_{\rm bin} p_T dp_T)]_{\rm central}}{[dN/(N_{\rm bin} p_T dp_T)]_{\rm peripheral}}. \tag{3}
$$

Here we use the same $N_{\rm bin}$ value as the STAR Collaboration at the corresponding collision centrality [3]. One can see in Fig. 2(a) that there are only slight differences for the $R_{\rm CP}$ of different particle species. This is because hadrons are produced from string fragmentation in the Lund model, and the fragmentation patterns for different particle species in central collisions and in peripheral collisions are set to be the same. We note that initial incoming nucleons can be transformed to proton and Λ via the associated production channel $N + N \rightarrow N + \Lambda + K^+$. Some of the particles are scattered into midrapidity region. As a result, $R_{\rm CP}$ of proton and
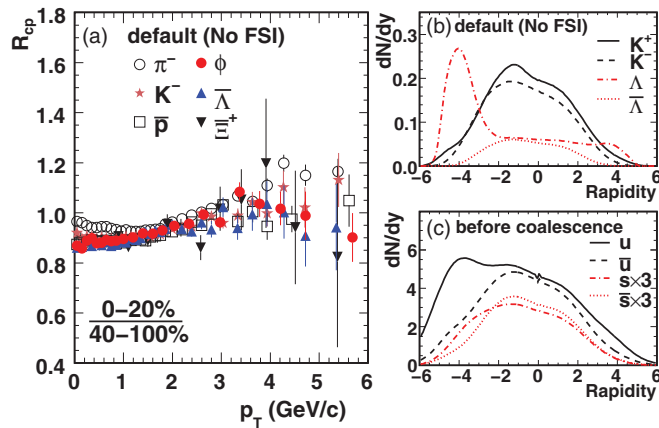
FIG. 2. (Color online) (a) R_{CP} for π^-, K^-, $\bar{p}$, ϕ, $\overline{\Lambda}$, and $\overline{\Xi}^+$ in d + Au $\sqrt{s_{NN}} = 200$ GeV collisions from default AMPT without the final state interactions included. (b) Kaon and Λ rapidity distribution in "minimum bias" d + Au collisions from default AMPT without the final state interactions included. (c) Quark (u, $\bar{u}$, s, and $\bar{s}$) rapidity distribution before coalescence in "minimum bias" d + Au collisions from string melting AMPT.

FIG. 3. Midrapidity R_{CP} ($|y| < 0.5$) in d + Au $\sqrt{s_{NN}} = 200$ GeV collisions from default AMPT with (solid circles) and without (open circles) final state interactions.

Λ would be larger at midrapidity even without the final state hadronic rescatterings included. One can see from Fig. 2(b) the enhanced production of Λ and K^+ with respect to their corresponding antiparticles ($\overline{\Lambda}$ and K^-) in "minimum bias" d + Au collisions. This is especially apparent for Λ close to the gold beam direction (gold beam rapidity: -5.36). The default AMPT calculation is consistent with STAR data on forward Λ production [17,22]. The strange quark enhancement in the large rapidity region (gold beam direction) will cause the corresponding increase of the $\bar{s}$ quark at other rapidity regions due to net strangeness conservation. This is shown in Fig. 2(c): the quark rapidity distribution before coalescence in "minimum bias" d + Au collisions from the string melting AMPT.

After including the final state hadronic interactions and strong decays of resonances, the R_{CP} of different particle species will change differently, as they have different masses and scattering cross sections. We show in Fig. 3 the comparisons of R_{CP} with and without the final state rescatterings and resonance decays. For π^- and K^-, the R_{CP} decreases after including the final state interactions from intermediate to high p_T. This suppression increases with p_T. Since most of the produced particles are pions at midrapidity, the scatterings are mainly the particle-pion interactions for $p \gg m_0$, where p and m_0 are the momenta and masses of corresponding particles, respectively. For π-π elastic collisions, the resonance peak centers at the position of π-π center-of-mass energy $\sqrt{s_{\pi\pi}}$ close to the ρ meson rest mass. Since most of the outgoing particles which probably scatter with each other are in similar directions, the open angle between two scattering particles is small. In our studied p_T and rapidity range, for one particle at low p_T, and another particle with higher energy, the calculated $\sqrt{s_{\pi\pi}}$ is closer to the resonance peak. In central collisions (0%–20%), the produced particles are several times more than the peripheral collisions (40%–100%), therefore the probabilities of the hadronic rescatterings are much larger. As
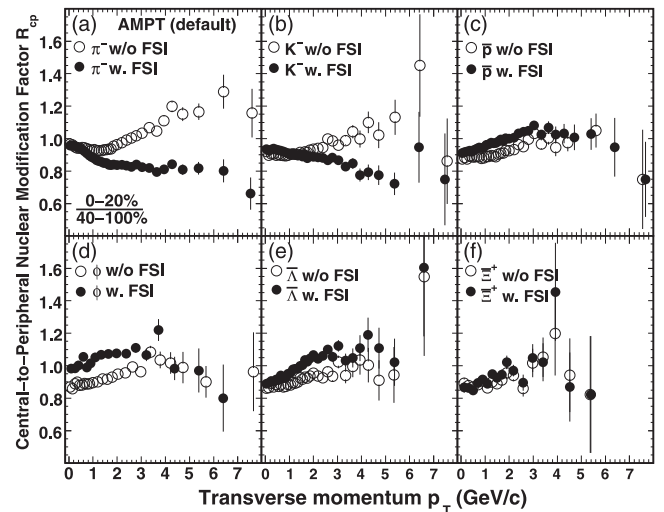
a result, this hadronic rescattering effect on R_{CP} is enhanced with increasing p_T for pions. A similar argument is also valid for K-π scatterings. For heavier particles such as the antiproton, ϕ meson, $\overline{\Lambda}$, the R_{CP} increases at low p_T according to their corresponding production channels or due to diffusions into the midrapidity region, but changes slightly for $p_T > 3$ GeV/c. We take antiproton-pion scattering as an example. If one chooses a pion momentum $p = 0.5$ GeV/c, with a small open angle between two scattering particles assumed as above (one assumes to be $10°$ here), the center-of-mass energies of antiproton-pion scattering are between 1.10 and 1.14 GeV for antiproton with momentum p between 1 and 6 GeV/c. The center-of-mass energies are away from the resonance peak position of antiproton-pion scattering, therefore the corresponding cross sections are much smaller compared to π-π scattering around the resonance peak. As a result, the effect of hadronic rescatterings is less apparent for the antiproton than for the pion. For even heavier particles, such as $\overline{\Xi}^+$, there is no obvious change of R_{CP} due to the final state interactions. Here particle mass plays an important role in the hadronic rescatterings. It will determine the space-time configuration of formed hadrons [24] as well as the center-of-mass energies and cross sections of subsequent hadronic rescatterings.

According to above analysis, the final state hadronic rescatterings will lead to particle mass dependence of R_{CP}. In Fig. 4, we compare the data with model calculations. At intermediate p_T, the R_{CP} of heavier particles like antiproton, ϕ meson, $\overline{\Lambda}$, $\overline{\Xi}^+$ will be larger than those of π^- and K^-. The result is qualitatively consistent with experimental data [3], as shown in Fig. 4(c). At intermediate p_T, the R_{CP} of antiproton is systematically larger than that of π^-. In Fig. 4(d), the ratio $R_{CP}(\bar{p})/R_{CP}(\pi^-)$ from the default AMPT model also agrees very well with experimental data. The year 2008 data of RHIC with higher statistics will provide more precise measurements and test our predictions for other hadron species such as the
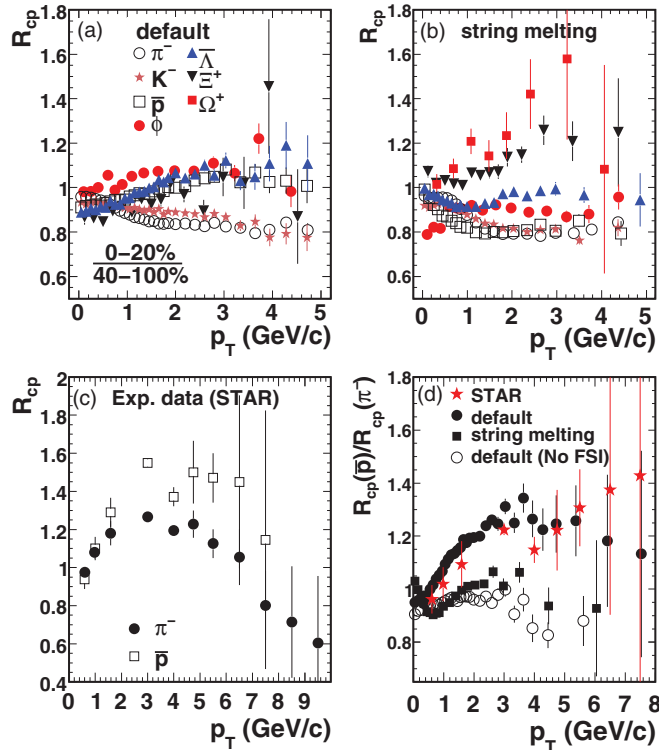
FIG. 4. (Color online) Midrapidity ($|y| < 0.5$) R_{CP} in d + Au $\sqrt{s_{NN}} = 200$ GeV collisions: (a) Default AMPT with final state interactions; (b) string melting AMPT with final state interactions; (c) experimental data of R_{CP} from the STAR Collaboration (statistical error only) [3]. (d) The ratios of $R_{CP}(\bar{p})/R_{CP}(\pi^-)$ from the STAR Collaboration, from default AMPT, from string melting AMPT, and from default AMPT without final state interactions.

ϕ meson, $\overline{\Lambda}$, $\overline{\Xi}^+$, etc. We note that the present calculation cannot reproduce the p_T dependence of R_{CP}. Possible issues associated with the initial condition such as gluon saturation [25–27], possible extra parton intrinsic p_T broadening [6–11], and so on are not addressed in this Rapid Communication. A future more complete analysis should take into account these effects.

For comparisons, the R_{CP} from string melting AMPT with quark coalescence is also studied. We have shown in Fig. 2(c) that the excess of the $\bar{s}$ quark over the s quark at mid-rapidity is partly due to associate production from initial multiple interactions. Combining this effect with the coalescence of partons, there are enhancements of corresponding hadrons at intermediate p_T. The R_{CP} values for different particle species that contain different numbers of $\bar{s}$ quarks are shown in Fig. 4(b). Note that multistrange hadrons are particularly interesting as they suffer much fewer hadronic interactions [28] compared with nonstrange hadrons. Therefore they are more sensitive to early-stage dynamics. At intermediate p_T, there is

an enhancement of R_{CP} according to the number of $\bar{s}$ quarks, that is, $R_{CP}(\overline{\Lambda}) < R_{CP}(\overline{\Xi}^+) < R_{CP}(\overline{\Omega}^+)$. Note that the values of R_{CP} for strange particles (Λ, Ξ, and Ω) are close to each other (not shown here) at the same transverse momentum region. If one assumes the validity of the coalescence approach, this observation shows that the measured R_{CP} can, to some extent, reflect the density of quarks shortly before the freeze-out. However, from the coalescence calculation the R_{CP} of the antiproton is close to that of π^- at intermediate p_T, which is not consistent with experimental data, as shown in Fig. 4(d) . This shows that the species dependence of R_{CP} also depends on the detailed properties of the system's evolution, for example, the initial multiple scattering between incoming nucleons and the hadron formation mechanisms.

In summary, we studied the mechanism of hadron formation and subsequent interactions in d + Au collisions at $\sqrt{s} = 200$ GeV. In a multiphase transport model with Lund string fragmentation for hadronization and the subsequent hadronic rescatterings included, we find a particle mass dependence of the central-to-peripheral nuclear modification factor R_{CP}. Recent data on particle species dependence of R_{CP} at midrapidity for d + Au collisions at RHIC can be understood in terms of this final state hadronic rescattering. This shows the importance of final state hadronic interactions in d + Au collisions, since none of the initial state models would predict a species-dependent R_{CP} at present. However, the calculations cannot reproduce the p_T dependence of R_{CP} with only final state interactions. Possible issues associated with the initial condition such as gluon saturation [25–27], possible extra parton intrinsic p_T broadening [6–11], and so on are not addressed in this Rapid Communication. A future more complete analysis should include these effects. In comparison, if the hadron is formed from quark coalescence, it is difficult to explain antiproton transverse momentum spectra and the particle species dependence of R_{CP}. On the other hand, the strangeness effect plays an important role in hadron production. This shows that the species dependence of R_{CP} also depends on the detailed properties of the system's evolution, for example, the initial multiple nucleon scattering and the hadronization mechanisms. More precision data in the future will test the findings in this Rapid Communication.

[1] J. W. Cronin, H. J. Frisch, and M. J. Shochet *et al.*, Phys. Rev. D **11**, 3105 (1975).

[2] D. Antreasyan, J. W. Cronin, and H. J. Frisch *et al.*, Phys. Rev. D **19**, 764 (1979).

[3] STAR Collaboration, J. Adams *et al.*, Phys. Lett. B **616**, 8 (2005); **637**, 161 (2006).

[4] S. S. Adler *et al.* (PHENIX Collaboration), Phys. Rev. C **74**, 024904 (2006).

[5] BRAHMS Collaboration, I. Arsene *et al.*, Nucl. Phys. A **757**, 1 (2005); PHOBOS Collaboration, B. B. Back *et al.*, *ibid.* **757**, 28 (2005); STAR Collaboration, J. Adams *et al.*, *ibid.* **757**, 102 (2005); PHENIX Collaboration, K. Adcox *et al.*, *ibid.* **757**, 184 (2005).

[6] M. Lev and B. Petersson, Z. Phys. C **21**, 155 (1983).

[7] G. Papp, P. Lévai, and G. Fai, Phys. Rev. C **61**, 021902(R) (1999).

[8] X. N. Wang, Phys. Rev. C **61**, 064910 (2000).

[9] I. Vitev and M. Gyulassy, Phys. Rev. Lett. **89**, 252301 (2002).

[10] B. Z. Kopeliovich, J. Nemchik, A. Schafer, and A. V. Tarasov, Phys. Rev. Lett. **88**, 232303 (2002).

[11] A. Accardi and M. Gyulassy, Phys. Lett. B **586**, 244 (2004).

[12] R. C. Hwa and C. B. Yang, Phys. Rev. Lett. **93**, 082302 (2004); Phys. Rev. C **70**, 037901 (2004).

[13] B. Andersson, G. Gustafson, and B. Söderberg, Z. Phys. C **20**, 317 (1983).

[14] B. Andersson, G. Gustafson, G. Ingelman, T. Sjöstrand, and X. Artru, Phys. Rep. **97**, 31 (1983).

[15] X. N. Wang and M. Gyulassy, Phys. Rev. D **44**, 3501 (1991).

[16] Z. W. Lin, C. M. Ko, B. A. Li, B. Zhang, and S. Pal, Phys. Rev. C **72**, 064901 (2005), and references therein.

[17] Z. W. Lin and C. M. Ko, Phys. Rev. C **68**, 054904 (2003).

[18] S. A. Bass, J. Phys.: Conf. Ser. **50**, 279 (2006).

[19] B. Zhang, Comput. Phys. Commun. **109**, 193 (1998).

[20] B. A. Li and C. M. Ko, Phys. Rev. C **52**, 2037 (1995).

[21] J. Adams *et al.* (STAR Collaboration), Phys. Rev. C **70**, 064907 (2004).

[22] B. I. Abelev *et al.* (STAR Collaboration), Phys. Rev. C **76**, 064904 (2007).

[23] B. I. Abelev *et al.* (STAR Collaboration), Phys. Rev. C **79**, 064903 (2009).

[24] K. Gallmeister and T. Falter, Phys. Lett. B **630**, 40 (2005).

[25] L. V. Gribov, E. M. Levin, and M. G. Ryskin, Phys. Rep. **100**, 1 (1983).

[26] A. H. Mueller and J. Qiu, Nucl. Phys. B **268**, 427 (1986).

[27] L. McLerran and R. Venugopalan, Phys. Rev. D **49**, 2233 (1994); **49**, 3352 (1994).

[28] H. van Hecke, H. Sorge, and N. Xu, Phys. Rev. Lett. **81**, 5764 (1998).